Solid-State Chemistry

International Edition: DOI: 10.1002/anie.201508381
German Edition: DOI: 10.1002/ange.201508381

Thinking Like a Chemist: Intuition in Thermoelectric Materials

Wolfgang G. Zeier, Alex Zevalkink, Zachary M. Gibbs, Geoffroy Hautier, Mercouri G. Kanatzidis, and G. Jeffrey Snyder**

Keywords:
band convergence · electronic structures · thermal conductivity · thermoelectrics

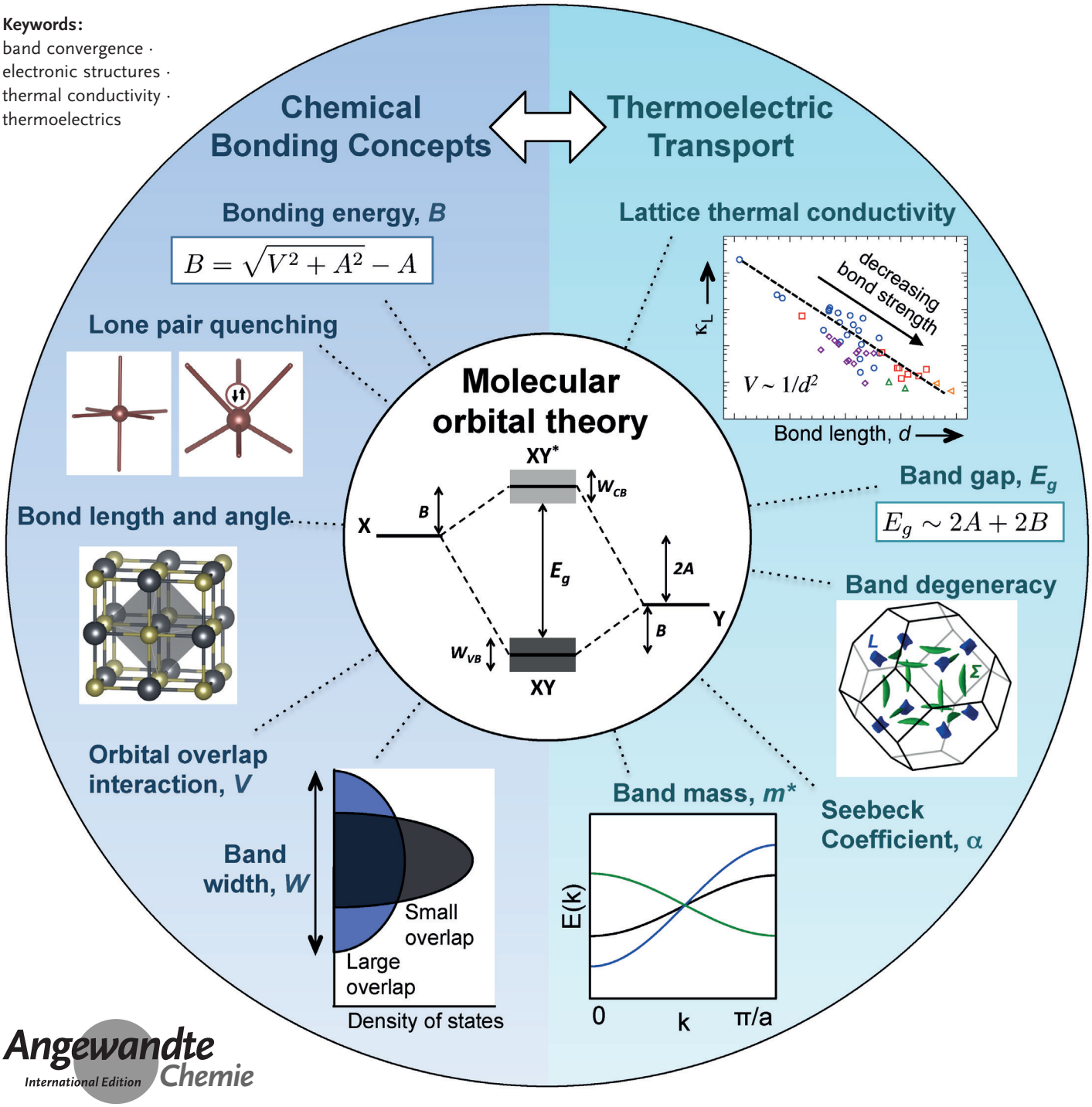

The coupled transport properties required to create an efficient thermoelectric material necessitates a thorough understanding of the relationship between the chemistry and physics in a solid. We approach thermoelectric material design using the chemical intuition provided by molecular orbital diagrams, tight binding theory, and a classic understanding of bond strength. Concepts such as electronegativity, band width, orbital overlap, bond energy, and bond length are used to explain trends in electronic properties such as the magnitude and temperature dependence of band gap, carrier effective mass, and band degeneracy and convergence. The lattice thermal conductivity is discussed in relation to the crystal structure and bond strength, with emphasis on the importance of bond length. We provide an overview of how symmetry and bonding strength affect electron and phonon transport in solids, and how altering these properties may be used in strategies to improve thermoelectric performance.

From the Contents

1. Introduction 6827
2. Chemical Bonding and Electronic Transport 6828
3. Chemical Bonding and Phonon Transport 6835
4. Summary and Outlook 6838

1. Introduction

Historically, the broad based implementation of thermoelectric energy conversion in commercial applications has been limited because of the low efficiency of thermoelectric materials.[1,2] Thanks to intense research efforts of the past decade, however, we have seen a doubling of thermoelectric efficiencies and a resurgence of commercial interest. Modern developments, such as an understanding of the effects of nanostructural engineering on the thermoelectric properties,[3,4] band engineering of lead chalcogenides,[5,6] superionic conductors,[7,8] and complex crystal structures,[9–14] to name a few, have all been utilized to further increase efficiencies. Comprehensive reviews of both historic and recent successes in the thermoelectric field can be found in the following sources.[4,5,13,15–24] Here we will discuss how simple chemical concepts can be turned into effective strategies for improving thermoelectrics and understanding complex semiconductor chemistry in general.

High thermoelectric efficiencies are found in materials with high Seebeck coefficients, α, high electrical conductivity, σ, (low electrical resistivity, ρ), and low thermal conductivity, κ. The thermoelectric figure of merit, or zT, combines these requirements into a single factor:

$$zT = \frac{\alpha^2\sigma}{\kappa_L + \kappa_e} T. \quad (1)$$

However, these properties are strongly coupled, making high zT values difficult to obtain in a straightforward way. The thermoelectric quality factor, β, is often preferred as a metric of a material's thermoelectric performance, because it distills the maximum attainable zT for a given material into its most fundamental material properties, assuming optimized carrier concentration. For the most common scattering type:[25]

$$\beta \propto \frac{N_V}{m_I^* \kappa_L}. \quad (2)$$

N_V is the valley degeneracy, m_I^* is the inertial effective mass along the conduction direction, and κ_L is the lattice thermal conductivity. A large valley degeneracy, low inertial effective mass and low lattice thermal conductivities will lead to high figure of merits.[26] Increased N_V means larger number of conduction pathways for charge carriers to participate in electronic transport,[17] while minimizing m_I^* improves electronic mobility ($\mu = \frac{e\tau}{m_I^*}$, where τ is the scattering relaxation time and m_I^* is the mass of the relevant band in the direction of electron transport).

The density of states effective mass m_{DOS}^*, is related to m_I^* through m_{band}^*:[5,19]

$$m_{\mathrm{DOS}}^* = N_V^{2/3} m_{\mathrm{band}}^*. \quad (3)$$

The density of states effective mass of a single valley (spherical Fermi pocket) has $m_{\mathrm{band}}^* = m_I^*$. For a given carrier concentration a high Seebeck coefficient can either be due to a large degeneracy, N_V, or a large m_{band}^*. While a large N_V will lead to a real increase of the quality factor and zT, larger m_{band}^* increases scattering and can ultimately be detrimental due to the relationship to m_I^* [Eq. (2)].

[*] Dr. W. G. Zeier, Prof. G. J. Snyder
Department of Materials Science and Engineering
Northwestern University
Evanston, IL 60208 (USA)
E-mail: jeff.snyder@northwestern.edu
Dr. A. Zevalkink
Max-Planck-Institut für Chemische Physik fester Stoffe
Nöthnitzer Strasse 40, 01187 Dresden (Germany)
Z. M. Gibbs
Division of Chemistry and Chemical Engineering
California Institute of Technology
Pasadena, CA 91125 (USA)
Prof. G. Hautier
Institute of Condensed Matter and Nanosciences (IMCN)
Université Catholique de Louvain
1348 Louvain-la-Neuve (Belgium)
Prof. M. G. Kanatzidis
Department of Chemistry, Northwestern University
Evanston, IL 60208 (USA)
E-mail: m-kanatzidis@northwestern.edu

These interdependent relationships illustrate the need to precisely control the fundamental properties in a material to optimize zT. While control of charge carrier concentrations can be straightforward via aliovalent elemental substitutions (i.e., doping) or by exploiting the intrinsic defect chemistry of the material,[27–34] the properties in β are not easily controlled without changing the underlying bonding interactions of the material. Ultimately, optimizing thermoelectric transport requires a comprehensive understanding of the fundamental properties such as the effective mass of carriers within a band, the band degeneracy, the band gap (to alter the influence of minority carriers),[35] as well as phonon velocity and phonon scattering. These are all heavily dependent on the structural chemistry of a solid and can therefore be considered from a chemical point of view.

In the following sections, we present a chemically intuitive approach to the key issues that govern thermoelectric materials. Central to this approach is a simplified model of a materials' band structure in the band gap region, which provides an intuitive understanding of how bonding affects electronic transport. Electronic transport and phonon interactions are then linked to concepts such as bonding character, bond strength and electronegativity. Through this approach, we attempt to use chemical intuition to provide a simple but powerful and qualitative perspective on thermoelectric transport and semiconducting solids in general.

2. Chemical Bonding and Electronic Transport

In the following section we address challenges such as how to engineer the effective mass of a band, the size of the band gap, and how to achieve band convergence by employing a simplified model for bonding and band structure evolution in the band gap region. For more in-depth discussions of the models employed here, the readers are referred to publications from Burdett,[36] Hoffmann[37] and Whangbo,[38] and, in combination with tight-binding theory, those from Rohrer[39] and Harrison.[40]

2.1. Simplified Bonding Model

Molecular orbital (MO) theory is a critical tool in chemistry to understand the bonding interactions of molecules. Here we consider a polar-covalent semiconductor with composition XY (see Figure 1); using a chemical picture, the MO is formed by the interaction of the atomic orbitals of element X and element Y, resulting in bonding XY and anti-bonding XY* molecular orbitals. In a solid, these molecular orbitals form bands, and the density of states can be directly inferred from the molecular orbital energies, as shown by Hoffmann.[37] In a 3D solid, a linear combination of such atomic orbitals (LCAO) can be used in a tight-binding method[40] to describe the electronic structure. The energy difference between the bonding and anti-bonding molecular orbitals (HOMO–LUMO gap in a molecule) in a solid is related to the band gap E_g between the valence and

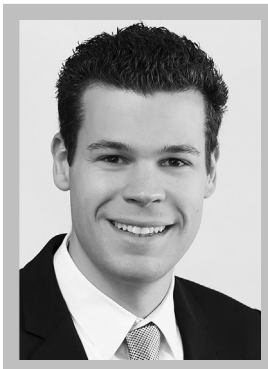

Wolfgang Zeier received his Ph.D. in Inorganic Chemistry in 2013 at the Johannes Gutenberg University in Mainz under the supervision of Prof. Wolfgang Tremel and Prof. Jeffrey Snyder. After postdoctoral studies at the University of Southern California and at the California Institute of Technology he was appointed junior group leader at the Justus Liebig University in Giessen. His research interests encompass the fundamental structure-to-property relationships in solids, with a focus on thermoelectric and ionic transport.

Dr. Alex Zevalkink received her B.S. from Michigan Technological University in 2008 and her Ph.D. under the supervision of Jeffrey Snyder at California Institute of Technology in 2014 with a focus on Zintl phase thermoelectrics. She has studied the electronic structure of skutterudite compounds as a NASA postdoc fellow at the Jet Propulsion Laboratory. Currently, she is pursuing high-pressure research as a postdoctoral fellow at the Max Planck Institute for Chemical Physics of Solids in Dresden.

Zach Gibbs is a Ph.D. Student at the California Institute of Technology with Jeff Snyder. He studies electronic transport physics in thermoelectric materials and has been working to develop electronic structure–property relationships with the goal of optimizing thermoelectric efficiency. He specializes in electronic structure characterization using a combination of optical, electronic, and computed properties coupled with semi-empirical transport models.

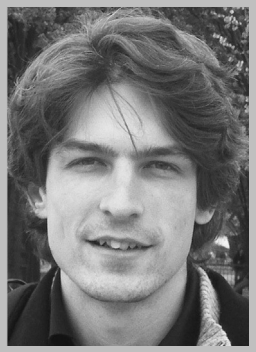

Geoffroy Hautier received in 2011 his Ph.D. from the Massachusetts Institute of Technology (MIT) with Professor G. Ceder. He worked afterwards as FNRS postdoctoral researcher and Marie Curie fellow in Professor X. Gonze's group at Université Catholique de Louvain (UCL). In 2014, he was appointed Assistant Professor in UCL. His research focuses on computational materials design and on high-throughput materials screening in various fields from Li-ion batteries to transparent conducting oxides and thermoelectrics.

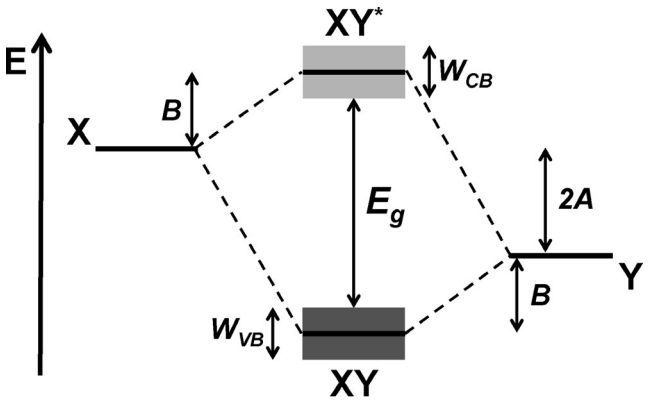

Figure 1. Molecular orbital (MO) scheme of the band and band gap formation in a solid with composition XY, with the energy difference 2*A* of the different atomic orbitals (X and Y), the width *W* (in energy space) of the conduction and valence band and the bonding energy *B*. The size of the band gap E_g is influenced by the different energy parameters *A*, *B* and *W*. XY and XY* are the bonding and anti-bonding MOs, respectively.

conduction bands. The band gap of the solid is related to the bonding parameters in Figure 1: $2A$ is the energy difference between the atomic orbitals, B is the strength of bonding interaction (i.e. bond energy), and W_{VB} and W_{CB} are the width of the valence and conduction bands, respectively.

The difference in the energies of the atomic orbitals, A, of X and Y can be essentially understood as the difference in ionization energy; the larger the ionization energy of an element, that is, higher electronegativity, the lower the energy of the atomic orbitals (Koopmans' theorem).[41] In a tight-binding approach, A represents the polar energy.[42] In Figure 1, for instance, element X exhibits a smaller electronegativity than Y, making X the cationic and Y the anionic species. As has been shown for a variety of materials,[43] a larger difference in EN between X and Y results in a larger band gap. In some cases, for example LiF (E_g = 13.6 eV) and KI (E_g = 6.3 eV) in the same structure type, the larger gap in LiF is entirely due to its larger A.

The electronegativity difference also influences the orbital character of the bands. For example, the anti-bonding state XY* in Figure 1 will have more X character, while the bonding state will have predominantly Y character. In the language of the linear combination of atomic orbital (LCAO) approach, the orbital coefficient of Y is larger than X in the XY bonding molecular orbital. The fractional character is related to the polarity of the bond (α_p) which can be described with $\alpha_p = A/\sqrt{V^2 + A^2}$. Thus a more ionic solid with a large A will ultimately have valence band states with primarily anion Y character and conduction band primarily of cation X character.[*] A more covalent material has nearly equal contributions of the X and Y atomic orbitals in both valence and conduction band.

The bonding energy B is the resulting energy from the stabilization of the molecular bonding orbital and destabilization of the antibonding orbital compared to the respective atomic orbitals. Whether considering a simple MO of a two atom molecule or a complete tight-binding approximation for a hetero-nuclear tetrahedral semiconductor the resulting bond energy can be expressed as:[39,40]

$$B = \sqrt{V^2 + A^2} - A, \tag{4}$$

with A as defined above, and V as the strength of nearest neighbor coupling (orbital overlap interaction). The first thing to notice is that interaction and mixing of atomic states always increases the energy separation of the resulting molecular orbitals. In general, the energy destabilization of the anti-bonding MO is slightly larger than the stabilization of the bonding MO, however, for simplification we neglect this as a second order effect. Intuitively, Equation (4) also shows that a large difference between the atomic orbital energies (larger A) will lead to weaker covalent bonding energy, B.

The orbital overlap interaction, V, is a combination of the interaction of all neighboring orbitals. Depending on the symmetry of the bonding interactions, it might include, for example, $V_{ss\sigma}$, $V_{sp\sigma}$, or $V_{pp\sigma}$, which are nearest neighbor interactions corresponding to s- and p-orbital σ-symmetric interactions.[40] As can be seen in Figure 2 a, a σ-bond between two p-orbitals will always result in a larger overlap than a π-

Mercouri Kanatzidis is a Professor of Chemistry and of Materials Science and Engineering at Northwestern University in Evanston. He also has a joint appointment at Argonne National Laboratory. His interests include materials for energy conversion, environmental remediation, and catalysis. He obtained his B.Sc. degree from Aristotle University in Greece, his Ph.D. from the University of Iowa, and was post-doctoral research fellow at the University of Michigan and Northwestern University. He holds a Charles E. and Emma H. Morrison Professor Chair at Northwestern University.

G. Jeffrey Snyder is a Professor of Materials Science and Engineering at Northwestern University in Evanston Illinois. His interests are focused on the materials physics and chemistry for thermoelectric engineering, such as band engineering, design of complex Zintl compounds and use of nanostructured composites. His interdisciplinary approach stems from studies of Solid State Chemistry at Cornell University and the Max Planck Institute for solid-state research, Applied Physics at Stanford University and thermoelectric materials & device engineering at NASA/Jet Propulsion Laboratory and California Institute of Technology.

[*] In large band gap insulators where electrons in such bands are not itinerant (not able to move freely), the electrons are localized and the band picture breaks down. For instance in NaCl the valance band is dominated by Cl^- 3p states, while the empty Cl 4s orbitals form the conduction band.[170]

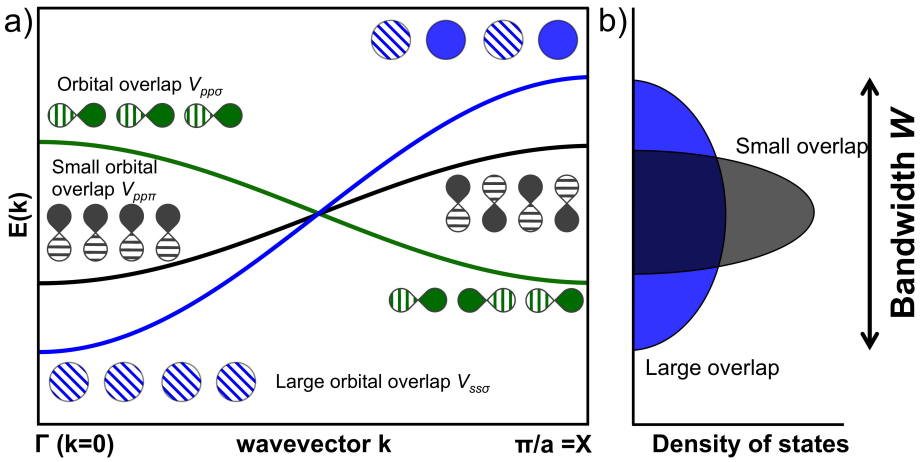

Figure 2. a) *E* versus *k* dispersion curves in the first Brillouin zone for a periodic array of s- and p-orbitals with σ and π type interactions. A stronger overlap due to σ interactions or smaller bond length leads to a broader separation between in-phase (bonding) at $\vec{k}=0$ and alternating phase (anti-bonding) orbitals at $\vec{k}=\pi/\alpha$ giving rise to a broader band dispersion. b) The broader dispersion leads to a lower density of states (3-D) and smaller effective masses of the charge carriers in the respective band.

bond. In all types of interaction, V decreases with increasing distance, d, according to

$$V \sim \frac{1}{d^2}. \tag{5}$$

Irrespective of principle quantum number (e.g., 3p, 4p and 5p), the valence shell interactions can be described by the same equation depending only on d.[40] Group 14 elements in the diamond structure provide an excellent example of how size, and by extension bond strength, influences the band gap in covalently bonded homo-nuclear solids ($A=0$), in which Equation (4) simplifies to $B=V$. The trend in band gaps of $E_g(C) > E_g(Si) > E_g(Ge) > E_g(\alpha\text{-Sn})$ follows from the decreasing orbital interaction (increasing d), which lowers the bond strength, and thus decreases the separation between the sp^3-bonding and sp^3-antibonding bands as one progresses from C to Sn.[44]

This general model using a tight-binding approach gives a reasonable description of the electronic structure for both covalent as well as ionic compounds, such that it serves as a useful starting point for most complex materials, which inevitably have a mixture of covalent and ionic character.

The width (or dispersion) of an electronic band W is critical in dictating the electronic properties in semiconducting materials. For example, increased W can reduce the band gap (see Figure 1) and if $W > B + A$, the states of XY and XY* will merge to form an overlapping band, resulting in a metal or semimetal.

The broadening of individual states into a band is the simplest interpretation of the bandwidth W. As shown schematically in Figure 2a for a chain of s-orbitals and p-orbitals, the broadening, and thus the width in energy space of the valence and conduction bands, increases with the degree of orbital overlap of neighboring molecular orbitals of the same energy. In Hückel theory, the bandwidth is described via the resonance integral, or transfer integral.[36] In a homonuclear solid ($A=0$), the bandwidth is determined by the overlap only via $W=4V$ (in the 1D),[44] with V corresponding to $V_{ss\sigma}$ in the case of a single σ-type interaction via s-orbitals, or $V_{pp\pi}$ for π-type interactions of p-orbitals.

Symmetric s-type interactions shown in Figure 2, which are fully bonding at $\vec{k}=0$ (Γ-point) and antibonding at $\vec{k}=\pi/\alpha$, result in a band topology with increasing energy in the direction of the Brillouin zone edge, that is, the band is running "uphill". On the other hand, p-type overlap-interactions will lead to decreasing $E(k)$ and a "downhill" topology (Figure 2).[37] However, in the tetrahedral, covalently bonded elements ($A=0$), tight binding shows the individual s- and p-states have broadened into a single valence band so extensively that the bandwidth is determined by the difference in energy between the s and p atomic orbitals, $\varepsilon_s - \varepsilon_p$ (see Figure 3).[39,40] In this tetrahedral case at Γ, the higher energy p-states in the valence band run down into the lower s-states, which are running up, resulting in an s–p bandwidth largely determined by s–p splitting, $\varepsilon_s - \varepsilon_p$ (Figure 3b-c). As bond length, d, decreases from grey-Sn to Ge, Si, and diamond-C, $\varepsilon_s - \varepsilon_p$ remains relatively constant, as does the bandwidth W. This explains why increasing B in this series can result in a strongly increased band gap.[44] Thus, despite the hybrid sp^3 state description being helpful in describing the structural chemistry it does not always completely describe electron energetics.

For polar compounds ($A \neq 0$), the band dispersion W will generally decrease with an increase in A, since the overlap, V, becomes less effective as the energy difference between neighboring orbitals increases. Thus, we can consider ionic materials as having large band gaps (E_g) and narrow bands (small W), in which charge carriers are heavy and easily localized.[39] In real space, it is perhaps intuitive to consider localized electrons as interacting with the lattice and each other, polarizing their surroundings as they move through the lattice. During transport, the polarization cloud moves through the lattice together with the electrons, resulting in "heavy", low mobility carriers.[44]

A narrow band (small dispersion) can thus result from factors such as longer bonds, a high degree of polarity, or f-orbitals, which have lower overlap than p- or s-interactions. A narrow band in energy space corresponds to a wide parabola in k-space, a large density of states (Figure 2b) and a high effective mass of the band, m^*_{band}. In contrast, a wide band in energy space (high dispersion) corresponds to a narrow parabola with low m^*_{band}, and is often expected in materials with small electronegativity differences (covalent bonds).[37,44]

The relationship between the above described properties and the electronic transport properties of semiconductors are

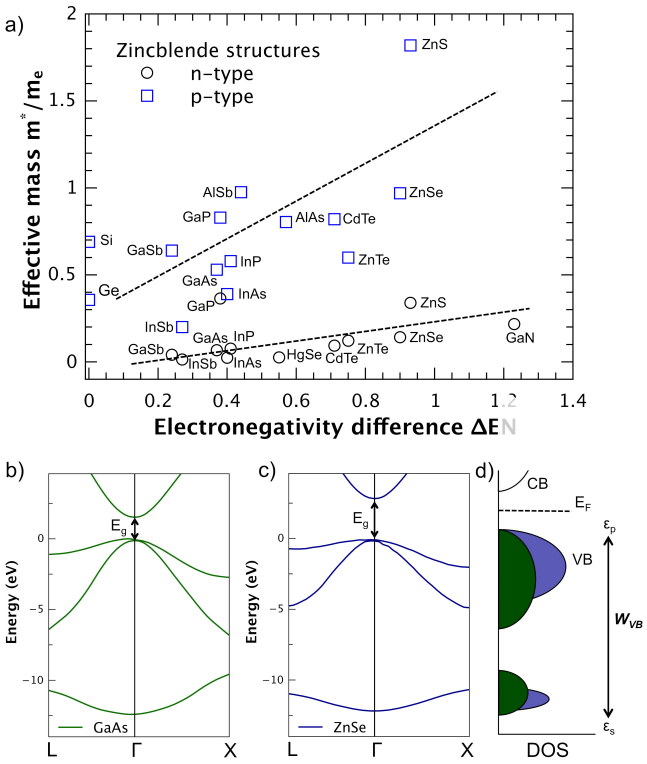

Figure 3. a) Increasing effective mass with increasing electronegativity difference ΔEN in tetrahedral covalently bonded materials in the zincblende structure. Valence band structure of GaAs (b) and ZnSe (c), calculated via tight binding,[46] showing the p-orbital character at the valence band edge. While the energy separation $\varepsilon_s - \varepsilon_p$ does not change significantly, the changing polarity A (ΔEN) leads to less disperse p-band resulting in an increase in the density of states (d) and therefore higher effective masses, which are detrimental for high charge carrier mobility. Data obtained from reference [45].

discussed in the following sections. It is evident, however, that a chemical understanding of bonding in solids using MO diagrams and tight binding is a powerful tool in understanding and predicting electronic band structure features without high level calculations being required.

2.2. Orbital Overlap and Effective Mass

The effect of increasing ionicity (or polarity) in covalent compounds is illustrated in Figure 3, which shows the influence of the electronegativity difference, ΔEN, on the band mass in compounds with the zincblende structure. With increasing ΔEN (larger A) there is a considerable amount of electron charge transfer between the ions,[45] and the effective masses of both the n-type and p-type materials increase due to a smaller dispersion of the band.[39]

This opens up the possibility to control and change the band effective masses of a material by altering the atomic basis states using solid solutions. For instance, in a more ionic solid, the valence band will be mainly comprised of anion states and a substitution of the anion will result in changes in the effective mass of holes. The effect of anion substitution on the thermoelectric transport has been shown in different solid solutions, for example, $PbSe_{1-x}S_x$, $(PbTe)_{1-x-y}(PbSe)_x(PbS)_y$ and $Cu_2ZnGeSe_{4-x}S_x$.[47–49] In these examples, substituting more covalent anions leads to better overlap in the valence band, leading to higher carrier mobility and altering band gaps (via different A). Recently it has been shown[50] that not only solid solutions, but even small concentrations of dopants can significantly reduce the mobility of charge carriers in their respective band. Therefore if p-type transport is desired, cationic dopants should ideally be used such that the valence band is not disrupted, and vice versa for n-type transport.[50] It is challenging to predict how the underlying chemical framework affects the scattering relaxation time τ, a comparison of effective masses and bonding interactions from material to material can therefore be powerful to understand and gauge electronic transport.

The relationship between bonding and carrier effective mass becomes more complex in ternary compounds with complex bonding schemes (i.e., various polyanions or different cation coordination environments) or strong hybridization of d- or f-orbitals with p-orbitals at the band edge.[51] For example, in Zintl phases, ionic and covalent bonding motifs exist in the same structure. Although determining the exact influence of these substructures on the band mass at the band edge may be difficult to predict, the relative ordering of the bands and the nature of the conduction and valence bands can be understood to a good extent using the above analysis.[9,20,29,52]

2.3. Temperature Dependent Band Gaps and Lone-Pair Effects

Although it is not directly included in the figure of merit, the band gap between the valence and conduction band plays a critical role in the thermoelectric performance of a material. When electronic carriers are thermally excited across the band gap, minority carriers begin to counteract the majority carriers and cause the thermopower to decrease and the thermal conductivity to increase due to bipolar conduction. E_g therefore determines the maximum useful operating temperature and the peak figure of merit.[54] Thus, controlling the band gap can be used to engineer both the figure of merit and the operating temperature range of a material.

Figure 4 compares the temperature dependence of E_g in semiconductors in the covalently bonded diamond structure with the more ionic lead rock salt chalcogenides. In most covalently bonded, tetrahedrally coordinated compounds (such as Si, Ge, InAs, GaAs, etc.),[53] an increase in temperature leads to decreasing band gap. In PbQ (Q = Te, Se, S) compounds, on the other hand, the opposite temperature dependence (and pressure dependence)[55] has been reported. This band gap increase, while at first glance perhaps unexpected, can be simply explained by a decreasing bandwidth in a material where the band gap is formed by the separation of atomic orbitals ($E_g \sim 2A$) with little contribution to the bonding ($B \sim 0$) as in an ionic compound.

In covalent, tetrahedrally bonded materials, the bandwidth is directly related to the energy difference of the s and p atomic orbitals, ε_s and ε_p, respectively (see Figure 3), which is nearly temperature independent.[39,40] Meanwhile, the

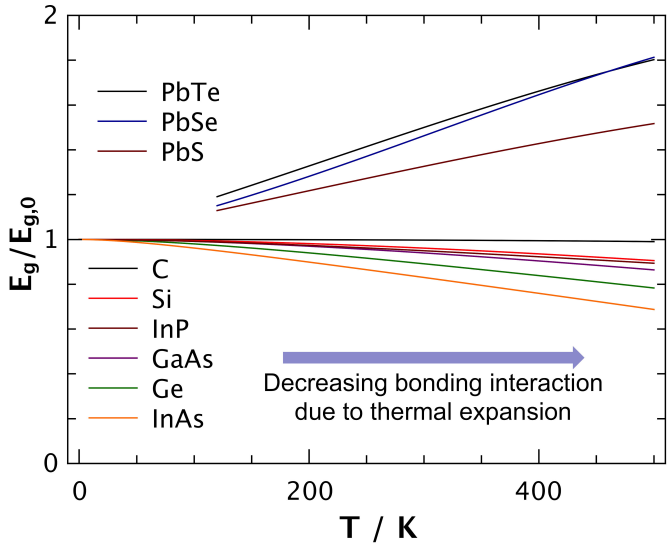

Figure 4. Temperature dependence of normalized band gaps $E_g/E_{g,0}$ of tetrahedrally coordinated covalent solids and lead chalcogenides.[53,54] Data curves are labeled and ordered from top to bottom. With increasing temperature, the interatomic distances increase due to thermal expansion. While E_g in tetrahedrally sp^3-bonded solid decreases, E_g for lead chalcogenides actually increases.

increase in bond length with temperature results in a decrease of the bond strength, B, (since $V \sim 1/d^2$) and concurrently the band gap, as seen in C, Si, Ge, and α-Sn. This can also be seen in other tetrahedrally bonded compounds such as the MQ family (where M = Zn, Cd, Hg; Q = S, Se, Te).

In the case of PbQ (Q = S, Se, Te), however, the valence band dispersion is influenced by the overlap interactions between the Pb and Q states (see Figure 6). An increase in the bond length due to thermal expansion results in a decrease of the orbital overlap, a smaller band dispersion, (decreased W_{VB}) and thus a shift of the valence band edge to lower energies, ultimately resulting in increased E_g. In these materials, the bonding interaction at a larger A is less influenced by the overlap V [see Eq. (4)].[44] Since materials generally expand with rising temperature, thus decreasing V, covalent semiconductors should exhibit decreasing band gaps, while ionic semiconductors should show increasing band gaps with temperature.

While calculations confirm[54] that simply increasing the unit cell size increases the band gap, in PbQ this is only half of the story. Particularly important is the involvement of the so-called s^2 lone pair orbital of Pb^{2+}. Experiments and calculations both show that the motion of the atoms in PbQ intensifies the increase in the band gap. This effect can be explained using the concept of "emphanisis" described by Bozin et al. for filled s-state elements such as Pb^{2+}.[56]

Emphanisis is the increase of local off-centering displacements of Pb^{2+} ions from a high-symmetry ground state upon warming. Such a phenomenon is unusual because, in the canonical view of structural transformations, a low-symmetry ground state evolves into a higher symmetry state on warming, while in PbQ the opposite is occurring. The Pb^{2+} off-centering is a dynamic, local, ferroelectric-like symmetry breaking that appears at increasing temperatures in the binary lead chalcogenides.[56,57] These materials, which were previously believed to adopt an ideal, undistorted rock-salt structure, appear to have locally distorted ones. Based on an intuitive argument discussed below, the emphanitic behavior of Pb^{2+} in PbQ may cause a lowering of the s^2 states near the top of the valence band and further contribute to the rising band gap with increasing temperature.

The so-called lone pair in main group elements of group 13, 14, and 15 is a dominant feature and plays a key role in the chemical properties of these elements and their respective compounds. The lone pair is formally from the s-valence electron pair (s^2), which tends to be more and more difficult to remove from the metal as we move down the respective group in the p-block elements. For example in group 13, the lone pair becomes increasingly stable as the element becomes heavier. Thus, it is more likely to be stabilized in In^+ than in Ga^+ and it is the most stable configuration for the heaviest Tl^+. The same applies to group 14 and 15 where the Pb^{2+} and Bi^{3+} possess very stable lone pairs; in fact, they are so stable that it is very difficult to remove these electrons to form Pb^{4+} and Bi^{5+} compounds, except for the very electronegative elements (F, O). The large stability of the s^2 pair in the heavier elements of the main group is attributed to relativistic effects that contract the size of the s-orbital and bring its electrons closer to the nucleus.

The s^2 lone pair behaves in unique ways depending on the local coordination environment. It can either stereochemically express itself by occupying its own distinct space around the metal atom or it can effectively "disappear" from view (we can refer to this as "quenched") when the metal adopts a perfect octahedral coordination. When it stereochemically expresses itself, there is a strong distortion around the metal atom and a lowering of structural symmetry.[58–61] The distortion lowers the energy of this orbital significantly.[62,63] From simple ligand field theory considerations, this happens because the repulsive forces from the surrounding ligands are lower than in the "quenched" case, in which the ligands do not allow any space for the s^2 pair to occupy. This is evident in the bond lengths of the ML_6 fragments illustrated in Figure 5. Specifically, for a given ML_6 fragment, if the lone pair is quenched, the M–L bonds in the octahedral environment (O_h) are longer than the M–L bonds in the distorted polyhedron with a stereochemically expressed lone pair and a [3+3] coordination. As the structure deviates and distorts from the ideal O_h towards an, for simplicity, arbitrary chosen C_{3v} symmetry state, the s^2 energy decreases. Whereas the actual orbital configuration changes slightly depending on the point group, this lowering in the s^2 energy occurs irrespective of the direction of the distortion.

It is interesting to compare the trends in compounds in which the s^2 pair either appears or is quenched. As the ligands bonded to M become heavier, there is a tendency for quenching and high local symmetry. This is seen in orthorhombic Bi_2S_3 versus rhombohedral Bi_2Se_3, orthorhombic SnSe versus cubic SnTe, rhombohedral GeTe versus cubic SnTe and in tetragonal PbO versus cubic PbS. In Bi_2S_3, GeTe, SnSe, and PbO the metal coordination is distorted and not octahedral. Simple size arguments via Pauling[64] do not explain the transitions to these crystal structures, in which the

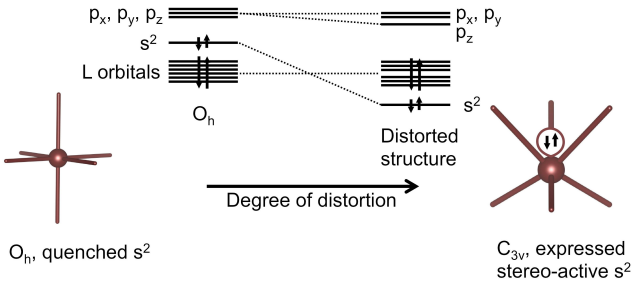

Figure 5. ML_6 fragments with M having an s^2 lone pair of electrons. In the octahedral form (O_h) the s^2 orbital experiences the highest repulsion from the *L* ligands and its energy is the highest occupied state. The p_x, p_y, p_z orbitals of M are the lowest unoccupied states. In the distorted C_{3v} symmetry, the L ligands adjust to make room for the lone pair stereochemical expression. This distorts the structure, lowers the ligand repulsions and stabilizes the s^2 state significantly. There is a continuum of energies since the lowering of s^2 orbital state energy increases with increasing degree of distortion.

lone pair of the metals is clearly expressed. In the very symmetric coordination environments of Bi_2Se_3, PbTe, SnTe, and PbS, the lone pair energy is raised and lies near or at the top of the highest occupied state. In a solid-state semiconductor, this will define the top of the valence band (Figure 6), just as it is the highest occupied state in the example of Figure 5.

The dilemma between being expressed or being quenched for the lone pair of Tl, Ge, Sn, Pb, Sb, and Bi has profound consequences in the structural and electronic properties of their compounds. For example, in semiconductors containing these elements, stereochemical expression increases the band gap as the s^2 stabilizes in energy (Figure 5). This explains why Bi_2S_3 has a band gap of 1.3 eV, when only about 0.5–0.6 eV would be expected had it adopted the higher symmetry rhombohedral Bi_2Se_3 structure type. We can point to many other examples; the band gaps of orthorhombic Sb_2Se_3 at 1.1 eV is quite high, while its tellurium analog Sb_2Te_3 has only 0.11 eV; alternatively orthorhombic SnSe has a gap of 0.8 eV, while in SnTe the gap is only 0.15 eV. In both cases Sb_2Se_3 and SnSe have distorted structures with expressed lone pairs of Sb^{3+} and Sn^{2+}, whereas Sb_2Te_3 and SnTe feature perfect octahedral coordination in their rhombohedral and cubic structures.

The anomalous band gap trends of PbTe, SnTe, and Bi_2Te_3, Sb_2Te_3 represent yet another consequence of the behavior of lone pairs. Generally, in analogous compounds the normal trend in energy gap is to decrease as the size and weight of the atom increases, due to an increasing overlap *V*. This is evident in the vast majority of semiconductors, which lack metals with lone pairs. However, the band gaps of SnTe and Sb_2Te_3 are smaller than those of PbTe and Bi_2Te_3 respectively. Why? The answer to this question lies in the energetic behavior of the s^2 lone pair. In the smaller Sn and Sb atoms, the energy of the s^2 is higher than that in Pb and Bi. This raises the top of the valence bands to higher energy narrowing the band gap. Furthermore with increasing temperature in PbQ, the stereochemical expression increases,[56] lowering the s-band in energy, resulting in an effective increase of the band gap.

An intuitive understanding of s^2 lone pair behavior can be exploited and combined with other trends described in this Review to create new ideas for engineering of novel thermoelectrics. Indeed, the increasing band gap with temperature in the lead chalcogenides (caused in part by lone pair expression) is one of the major reasons why these materials are good thermoelectric materials at high temperatures, due to suppressed bipolar conduction as well as converging bands (see

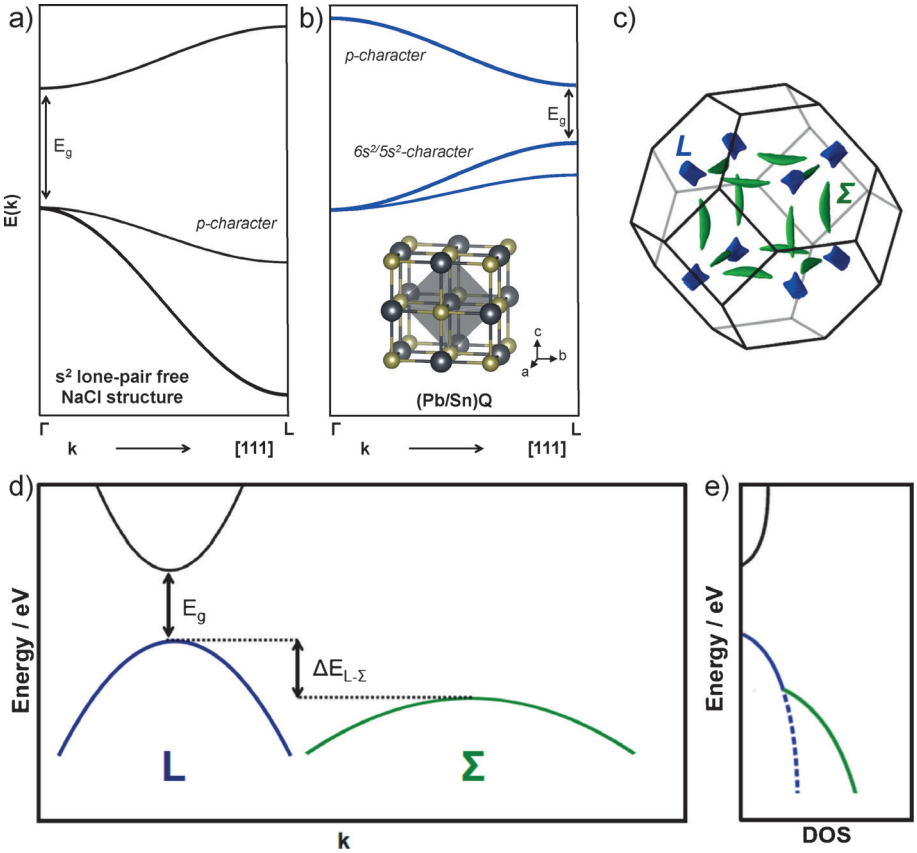

Figure 6. Band diagram at the band edges for a) Pb/Sn-free compounds in the rock salt structure and b) Pb and Sn chalcogenides. Whereas in (a) the band maximum is at Γ with a p-band running down in energy towards the *L* point, in (b) the lone pairs $5s^2$ and $6s^2$ lead to a predominant s-character of the valence band and a band maximum at *L*. c) The Brillouin zone for space group $Fm\bar{3}m$ with the Fermi surfaces for the pockets of the L and Σ valence bands. d) Energetic band configuration and DOS (e) of the L and Σ bands for SnTe and PbTe. If the energy separation, $\Delta E_{L-\Sigma}$, becomes small (1–2 k_BT around E_F), beneficial band convergence occurs. $\Delta E_{L-\Sigma}$ for Sn compounds is larger due to less contracted $5s^2$ orbitals, resulting in a stronger overlap and a broader band.

Figure 6). Further examples of controlling band gaps include Zintl compounds $Ca_5M_2Sb_6$ (M = Al, Ga, In),[29] where the differences in the electronegativity lead to changes in the band gaps and ultimately the electronic mobility, and $AgBiSe_2$, where doping with the more ionic halide anions has also shown to be successful for changes in E_g.[65]

2.4. Complex Fermi Surfaces: Valley Degeneracy, Anisotropy, and Band Convergence

High valley degeneracy, N_v, is a key factor for good thermoelectric materials, as demonstrated by the quality factor given in Equation (2). A multi-valley Fermi surface requires the conducting Fermi surface pockets to be at low symmetry positions, preferably shifted slightly away from the Γ-point (the zone center). Band extrema occurring exactly at the Γ point have the lowest possible N_v and are thus less desirable.[66] The increased conductivity from multiple pockets can be thought of as having a higher Fermi surface area for the same Fermi surface volume. Anisotropic Fermi surfaces[67] (even in cubic materials) or interconnected threads[68–71] of Fermi surface can have the same effect and increase the quality factor by increasing the mobility (reducing the conductivity effective mass, m_I^*).[72] Complex Fermi surfaces can also be exploited in anisotropic materials, in which the high mobility direction (low m_I^*) is likely to be the best for thermoelectricity.[66]

Unfortunately, the most common ionic configuration—conduction bands with cation s-like character and valence bands with anion p-like character—typically results in a direct gap semiconductor at the Γ-point (Figure 6b). As described in Figure 2, this is because s-like interacting states run up from Γ, while p-like states tend to run down from Γ. In MgO (NaCl structure), for example, the valence band is comprised of O-2p states, which, due to their $V_{pp\sigma}$ interaction, exhibit a decrease in the band along Γ to L, i.e., in the [111] direction. The conduction band is mostly Mg 3s states and runs uphill as seen in Figure 2. This leads to a direct band gap at Γ, which is indeed observed in most rock salt materials.

In the Pb^{2+} and Sn^{2+} compounds, however, the cation s^2 lone pair changes the character of both bands and moves the gap away from Γ. The filled s^2-lone pair is energetically located at the top of the valence band and leads to a bonding situation at Γ and anti-bonding at L. In other words, the lone-pair configuration leads to a valence band at L with predominantly s-orbital like character (see Figures 5 and 6a). This is distinct from the Σ band, which has anion p-character (see partial DOS Figure 7).[73] This also explains why the energy gap $\Delta E_{L\text{-}\Sigma}$ is larger for SnTe than for PbTe, since the s-state of Sn is at a higher energy.[74–76] With the cation s-states filled and far away from the cation p-states in energy, the conduction band edge has primarily p-orbital cation character so that it drops from Γ to L, producing a direct band gap at L with $N_V = 4$, instead of at Γ. This unique band behavior due to lone pairs can also be seen in transparent conducting oxides, where the highest hole mobilities are achieved in s^2 based materials, which are not limited to the low mobility of a O-2p band.[77]

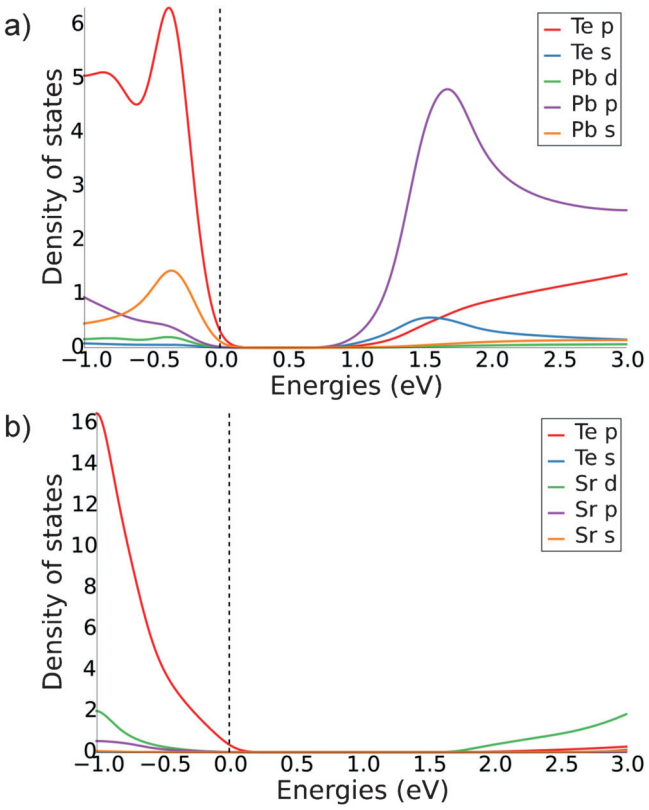

Figure 7. Calculated orbital projected partial density of states (DOS) of a) PbTe and b) SrTe at the valence and conduction band edge. Due to the lower electronegativity difference in PbTe, Pb s-states can be found in the valence band edge (Γ to L band). The interactions between Sr^{2+} and Te^{2-} are less covalent and the valence band is therefore mainly composed of Te states. Computations are from the Materials Project database[79] and use density functional theory within the generalized gradient approximation (GGA) in the Perdew–Burke–Ernzerhof (PBE) formulation without spin–orbit coupling (SOC).[80] SOC can be important with heavy elements such as Te and Pb but do not modify our discussion on projected DOS.

The valence band along the Σ line in lead chalcogenides has a valley degeneracy of $N_V = 12$, which is thought to be responsible for the exceptional thermoelectric properties in heavily doped p-type samples.[6] The twelve elongated Σ pockets form separately from the four L pockets (Figure 6c). With increasing temperature, the valence band at the L point (see Figure 6) moves to within a few $k_B T$ of the Σ band, leading to band convergence (separate bands with minima at the same energy) and an increase of the effective valley degeneracy. Thus, while it is difficult to change the N_V of a given compound (since this would mean a change in symmetry and crystal structure), a convergence of the valence bands allows for a larger combined N_V (see Figure 6d,e).[6,17,78] In the case of PbTe, two valence bands converge at ~700 K,[54] leading to an effective band degeneracy of 12–16 and high figure of merit.[6]

Band convergence can be engineered via substitution with cations such as Sr^{2+} and Mg^{2+} in PbTe,[3,81] and PbSe.[82,83] Substitution of Pb with Sr leads to an increase in the band gap between the L valence band and the conduction band, which

concurrently lowers the energy gap $\Delta E_{L\text{-}\Sigma}$. This can be understood by comparing the calculated density of states at the band edge for PbTe and SrTe (Figure 7). The smaller electronegativity difference between Pb and Te (smaller A), and the presence of the lone pair, leads to a contribution of Pb states in the valence band. However, the more ionic SrTe (larger A, larger E_g) behaves more like a purely ionic system, in which the valence band is comprised mostly of Te p-states, exhibiting the valence band maximum at Γ. Substitution of Pb with Sr results in a higher effective polarity, A, leading to a perturbation in the dispersion of the lone pair band (W_{VB}) and hence an increase in the band gap (see Figure 2c,d)). This shifts the L band closer to the Σ band, leading to a more effective band convergence and ultimately a higher figure of merit. Since the bands at Σ are Te-p in character, a substitution on the cation site does not lead to any significant changes in these bands. The approach of substitution with a more electropositive cation has also been successful in improving the band convergence in Mg-doped PbTe[84] and Hg/Cd doped SnTe.[75,76,85] Computationally, Zhu et al.[86] have explored influencing band convergence via changes in orbital interactions of solid solutions of binary chalcogenides, providing new pathways to high thermoelectric efficiencies. The compositional influences on the band convergence in materials like chalcopyrites[87,88] and Mg_2Si-Mg_2Sn[89,90] have already been confirmed experimentally.

3. Chemical Bonding and Phonon Transport

To achieve a high thermoelectric figure of merit, a low lattice thermal conductivity, κ_L, is essential. Reducing κ_L, caused via phonon propagation, has been one of the main focuses of thermoelectric research in recent decades. For a comprehensive overview of micro- and nanostructuring in thermoelectrics the reader is referred to reviews by Kanatzidis and co-workers.[21,26] The heat transported by electrons is easily estimated from the electronic conductivity thanks to the Wiedemann–Franz law ($\kappa_e = L\sigma T$) unless there is significant bipolar contribution. The Lorenz factor, L, typically does not vary by more than 20% from the value that can be estimated from the Seebeck coefficient.[91] Here, we focus on understanding the influence of chemical bonds on the phonon transport, κ_L, which can provide us with simple and intuitive strategies for thermoelectric materials.

3.1. Bond Strength

There have been several approaches to quantifying the influence that readily available, intrinsic materials parameters (e.g., crystal structure, elastic constant) have on κ_L. As an extension from the early work of Schlöhmann,[92] and more recently by Slack,[93] Klemens,[94] Julian,[95] and Toberer[96] focusing on acoustic phonons has shown that the influence on κ_L of the average mass, M, the elastic constants via the mean speed of sound, v_m, and the Grüneisen parameter, γ, the average volume per atom, V, and the number of atoms per primitive unit cell, N, can be written as:[96]

$$\kappa_L \sim \frac{M v_m^3}{T V^{2/3} \gamma^2} \left(\frac{1}{N^{1/3}}\right) \quad (6)$$

Increasing N in a material intuitively creates a more tortuous transport path for phonons, ultimately reducing κ_L by increasing phonon scattering opportunities and slowing short wavelength phonons. As N becomes very large, i.e., a completely amorphous material, the speed of sound becomes the most important characteristic and the thermal conductivity approaches a constant value, often called the minimum thermal conductivity:[97]

$$\kappa_L \sim 1.2 \frac{k_B v_m}{V^{2/3}} \quad (7)$$

Beyond Equations (6) and (7), there have been a number of other empirical approaches to provide intuition for κ_L. For example, observations by Ioffe et al.[98] show a decrease of the thermal conductivity with an increase of the ionicity of the bonds between the atoms, and Spitzer[99] showed a correlation between increasing coordination number (CN) in a crystal structure and decreasing lattice thermal conductivity. These largely qualitative relationships have proven invaluable in the search for and development of thermoelectric materials with low lattice thermal conductivity. Although perhaps not obvious at first glance, these relationships have a common underlying theme: they relate the lattice thermal conductivity to the strength of the chemical bonds in a material. In the following section, we will try to provide the reader with an intuition of how exactly bond strength, and thus κ_L, are informed by the character of the chemical bonds, using the average crystallographic bond length as a simple metric.

The dependence of the lattice thermal conductivity on the speed of sound is illustrated in Figure 8 for binary compounds with the zincblende structure (T_d symmetry, CN = 4) and rock

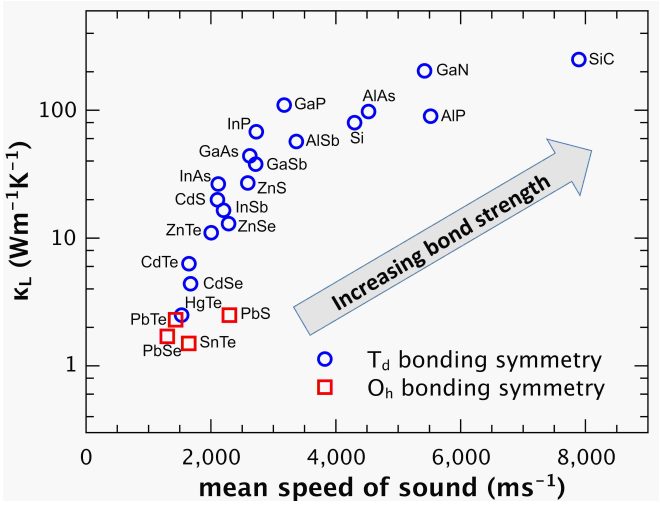

Figure 8. Dependence of κ_L on the average speed of sound in typical binary materials with the zincblende structure (T_d symmetry, $CN = 4$) and rock salt structures (O_h symmetry, $CN = 6$). Increasing bond strengths lead to an increase in the speed of sound, ultimately increasing the lattice thermal conductivity. The data were obtained from references [78, 93, 96, 98, 99, 101–123].

salt structures (O_h symmetry, CN = 6). The v_m dependence of κ_L can easily be understood by considering a simplified picture of the lattice as atoms (with mass M) connected by bonds (with spring constant k). The speed of phonons (waves) propagating through this lattice is given by the speed of sound, $v_m \sim \sqrt{k/M}$.[100] Intuitively, solids with lower bond strength, related to k, and heavier atoms exhibit slower speeds of sound. While the atomic mass of a material is easily determined, the bond strength is slightly less straightforward, since it is intimately linked to the size and mass of the atoms and the chemical nature of the bonds.

The elastic constants of a solid, for example, the bulk modulus, depend on the strength of the bonding interactions. Empirical calculations show that an increase in the bond length leads to a decrease in the bulk modulus in compounds, due to softening of the chemical bonds.[105,124] Furthermore, Downs and co-workers,[125] as well as Hoffmann and Ashcroft,[126] argue that the compression of a chemical bond by increasing external pressure on a solid makes it simultaneously more covalent and stronger. Therefore, the bond length can be used to gauge the strength of the bonding interaction in semiconductors, as has already qualitatively been shown for oxides.[127] Stronger bonding interactions (i.e., short bond lengths) increase the speed of sound, which in turn increases the lattice thermal conductivity. This is illustrated by Figure 9, which shows the lattice thermal conductivity of various binary and ternary semiconductors in the zincblende, rock salt and CsCl structure as a function of the average crystallographic bond length.

Since the bond strength can also be correlated with ionicity and coordination number, the observed dependence of κ_L on these terms by Ioffe[98] and Spitzer[99] can be explained. An increasing coordination number usually leads to an increase in the interatomic distance, due to the electrostatic repulsion in the lattice. Generally, more ionic compounds tend to crystallize in high coordination symmetries due to higher Madelung constants,[44] leading to longer bond lengths and therefore lower κ_L. In addition, the relationship between melting temperature and lattice thermal conductivity,[136] also stems from bond strength, since lower bond strength usually results in a lower melting point of a solid.

Recently Lee et al.[137] have correlated the differences in lattice thermal conductivities with the bonding interactions in the rock salt and zincblende structures of various thermoelectric compounds. Resonant bonding interactions seemingly lower the lattice thermal conductivity in the rock salt structures compared to tetrahedrally bonded structures. However, as Pauling's second rule states that bond strength decreases with coordination number,[138,139] this trend is ultimately related to the average bond length of the materials. This makes intuitive sense since tetrahedral coordination represents a tighter packing of atoms in the lattice than does octahedral or higher coordination, and tight packing implies a stiffer lattice and thus higher phonon velocities. In short, "soft lattices" are those where the atoms possess, on average, high coordination numbers for example, six or higher. In these structures phonon velocities tend to be very low, inhibiting heat propagation.

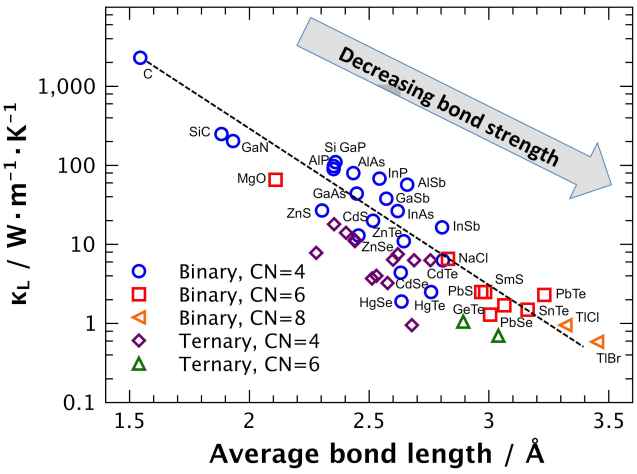

Figure 9. Lattice thermal conductivity decreases with average crystallographic bond length in binary and ternary compounds in the zincblende (*CN* = 4), rock salt structures (*CN* = 6) and CsCl structure (*CN* = 8). The broken line serves as a guide to the eye. Decreasing bond length directly leads to an increase in the bond strength and thus increased v_m. The higher coordination numbers in rock salt and CsCl structures leads to longer bonds and thus lower κ_L. References [98, 99, 108–110, 112–123, 128–135] were used to obtain κ_L, and average bond lengths are from the Inorganic Crystal Structure Database (ICSD).

3.2. Anharmonicity

While the average bond length in a material provides an intuitive measure to estimate the lattice thermal conductivity, it fails to account for anharmonicity of the lattice vibrations. In some compounds, low κ_L is primarily due to high Grüneisen parameters [Eq. (6)], which is a measure of the anharmonicity of the lattice vibrations.[140] Variations in the Grüneisen parameters, γ, likely account for some of the spread in Figure 9.[141] The Grüneisen parameter is defined as the change of the phonon frequency as a function of volume and depends on the thermal expansion coefficient, α_T, the volume V, the heat capacity C_V and the bulk modulus G, according to $\gamma = \frac{\alpha_T G V}{C_V}$.[140]

How can anharmonicity be understood in chemical terms? It is a measure of the asymmetry in the ability of an atom to vibrate harmonically around its position. Asymmetry in vibration implies the ability of the atom to move along certain directions of the lattice without causing large repulsions in its environment and destabilization of the entire structure. Such asymmetry is likely to be observed in either soft lattices or in lattices that are not well packed and have some room for the anharmonic atoms to engage in asymmetric vibrations and movement. Figure 10 shows a series of asymmetric bonding situations; the greater the anharmonicity, the larger the Grüneisen parameter of the system.

The Grüneisen parameters for some selected binary compounds can be found in Figure 11, which shows the γ^{-2} dependence of κ_L [Eq. (6)]. In general, solids with higher coordination numbers exhibit higher anharmonicity, which

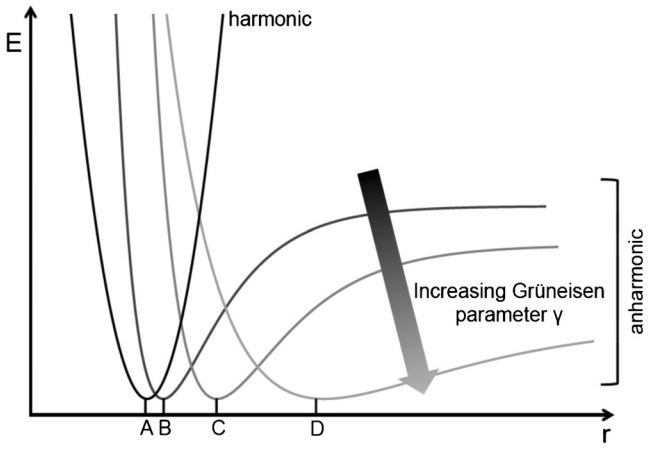

Figure 10. Anharmonic potential energy curves for four types of hypothetical atoms in a structure interatomic distance, *r*. Curve A represents a light atom with ideal harmonic motion. Curves B, C, D represent atoms with increasing size and mass, exhibiting increasingly anharmonic behavior. Keeping all other parameters constant, the structure, which contains atom D, will have the lowest κ_L.

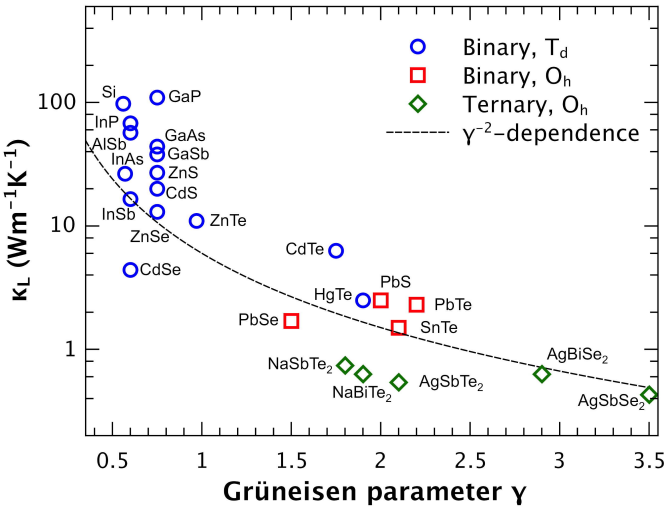

Figure 11. Influence of γ on κ_L in compounds with the zincblende (T_d) and rock salt structure (O_h). Most materials in tetrahedral symmetry have low γ. Materials with a higher atomic number *Z* and octahedrally coordinated structures exhibit higher γ. References [78, 93, 96, 99, 101–104, 106, 107, 143] were used to obtain γ and κ_L data.

leads to larger Grüneisen parameters for the rock salt compared to the zincblende structures.[142] Note that most materials in tetrahedral local environment have similar low γ for this reason. The high anharmonicity in ABX_2 compounds in the rock salt structure, in contrast, has been extensively investigated theoretically and experimentally by Nielsen et al.[143] (see Figure 11).

Materials with a higher atomic number, *Z*, also exhibit higher Grüneisen parameters, possibly due to contracted *s*-orbitals. Since anharmonicity can arise from local distortions in the atomic environment, the loss of inversion symmetry due to the lone pair configuration alters the thermal expansion and hence the Grüneisen parameter.[143] A similar behavior of the Grüneisen parameters has been found by Skoug and Morelli in materials with antimony lone pairs.[144,145] Taking this one step further, Wolverton and coworkers confirmed theoretically that the stereochemical activity of the lone pair influences the anharmonicity of the lattice in Cu_3SbSe_4, $CuSbSe_2$, and Cu_3SbSe_3, leading to anomalously low lattice thermal conductivity in these Cu-Sb-Se ternary semiconductors.[146] The structural distortion due to the lone pair is also an important factor leading to the anomalously large Grüneisen parameter in SnSe.[147]

3.3. Phonon Scattering via Site Disorder and Chemical Strain

An alternative approach to achieving low lattice thermal conductivity is to decrease the phonon mean free path by introducing additional scattering sources from defects and microstructure. The use of enhanced boundary scattering due to nanostructuring, interfaces or larger grains has been shown to scatter low frequency (large wavelength) phonons, reducing the phonon mean free path and achieving low κ_L.[4,148–154] At the opposite extreme, point defect scattering (or alloy scattering)[155] is an effective way to scatter high frequency phonons, which are usually not heavily scattered by phonon–phonon interactions.[151,155,156] Point defect scattering has been successfully implemented in almost every class of thermoelectric material, including Heusler compounds,[157] skutterudites,[158,159] lead telluride,[160] and $Si_{1-x}Ge_x$, among others.[111,161] This scattering mechanism relies on both *mass* field fluctuations and *strain* field fluctuations.[162,163] For example, in $Si_{1-x}Ge_x$ alloys[111,161] and in the $Ca_{1-x}Yb_xZn_2Sb_2$ Zintl phase[164,165] large mass contrast plays the central role in lowering the thermal conductivity. However, in some materials, the structural chemistry and local bonding environment play the most significant role.

For example, in the solid solution $Cu_2ZnGeS_{4-x}Se_x$, the lattice thermal conductivity is reduced primarily by strain due to large local disorder.[166] Within this solid solution, differences in the ionic radii and bonding strengths between Se and S lead to changes to the bond lengths and bond angles (see Figure 12). In general, variations in the bonding interactions through different bond strengths, bond lengths and bond angles can be expected to alter the local bulk modulus, ultimately increasing strain field fluctuations and hence the scattering by point defects.[167]

The effect of the bond strength and bond angles on κ_L was initially investigated in this class of materials by studying the solid solution $Cu_2Zn_{1-x}Fe_xGeSe_4$,[168] and further in $Cu_{1-x}Fe_{1+x}S_2$.[169] These represent materials containing non-special crystallographic positions, in which the use of local structural strain to enhance phonon scattering is a particularly promising approach. In contrast, if only special positions were present, the bond angles would not be allowed to change and no significant contribution to scattering via strain would be expected. This alloying approach not only provides the opportunity to alter the thermal properties, but also can enhance the electronic properties through careful selection of the alloying elements.

Finally, strain can also be introduced via nanostructuring with second phases. The endotaxial placement of nanocrystals

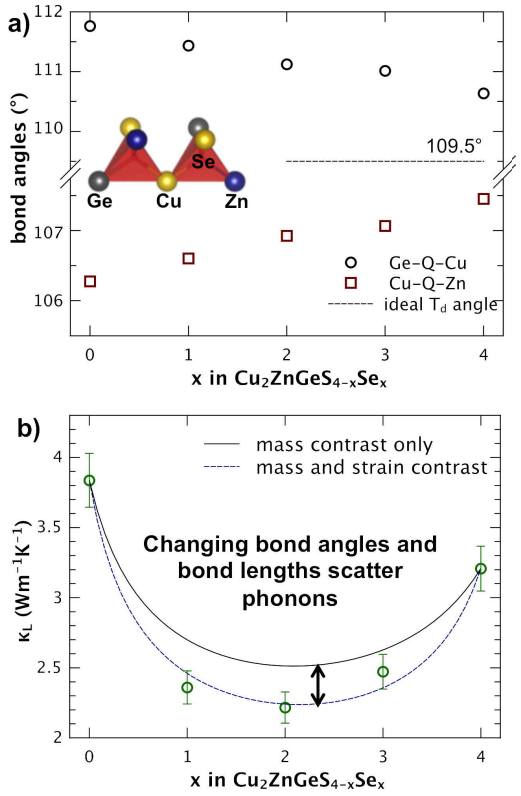

Figure 12. a) Selected Cu-Q-Zn and Ge-Q-Cu (Q = S, Se) bond angles of $Cu_2ZnGeS_{4-x}Se_x$. The inset shows the tetrahedral connectivity of these chalcopyrite structures. Due to the differences in ionic radii and bonding interactions, substitution of S with Se leads to a change in the bond lengths and bond angles. b) To explain the reduction of lattice thermal conductivity due to alloying, the mass contrast between Se and S and resulting strain from the changing structural arrangements must be accounted for.[166]

in a matrix material can create larger strain at the interfaces as the two structures try to lattice match to lower their free energy. The bonding at the interface can also create dislocations causing further strain. These phenomena are discussed in detail in the following reviews.[23,24]

4. Summary and Outlook

A simplified picture of the interactions that contribute to the electronic energies in a molecular orbital framework gives us the basic tools we need to describe critical electronic parameters such as band gap, band mass, and band degeneracy. The simple understanding of how bond distance affects electronic and thermal transport properties for example can explain the influence of the ionicity and coordination number on thermal transport: Larger bond length implies weaker bonding, a softer and more anharmonic lattice that leads to lower lattice thermal conductivity. Trends in physical properties due to alloying can be explained by considering the variation in the covalency, bond length, and bond strength of a material, as well as leading to local structural strain and disorder. A full understanding of s and p-types of bonding interactions, especially in materials with s^2 lone pairs, further enhances our understanding of the electronic structures and the chemical effects of alloying.

The chemical approach of thinking about local bonding interactions is a very powerful tool that can provide insight and new strategies for improving and finding new materials for thermoelectrics or other semiconductor applications.

Acknowledgments

W.G.Z. and G.J.S. acknowledge support from the Solid-State Solar-Thermal Energy Conversion Center (S3TEC), an Energy Frontier Research Center funded by the U.S. Department of Energy, Office of Science, Basic Energy Sciences under Award no. DE-SC0001299. The theory and density of states calculations for this project were performed under the Materials Project work, supported by Department of Energy Basic Energy Sciences program under Grant No. EDCBEE, DOE Contract DE-AC02-05CH11231. We thank Dr. Gregor Kieslich (Cambridge University) and Riley Hanus (Northwestern University) for the insightful comments and discussion. G.H. thanks for financial support from the European Union Marie Curie Career Integration (CIG) grant HTforTCOs PCIG11-GA-2012-321988. M.G.K. acknowledges support from the Department of Energy, Office of Science Basic Energy Sciences grant DE-SC0014520.

How to cite: *Angew. Chem. Int. Ed.* **2016**, *55*, 6826–6841
Angew. Chem. **2016**, *128*, 6938–6954

[1] C. B. Vining, *Nat. Mater.* **2009**, *8*, 83–85.
[2] D. M. Rowe, *Thermoelectrics Handbook. Macro to Nano*, CRC, Boca Raton, **2006**.
[3] K. Biswas, J. He, I. D. Blum, C.-I. Wu, T. P. Hogan, D. N. Seidman, V. P. Dravid, M. G. Kanatzidis, *Nature* **2012**, *489*, 414–418.
[4] A. J. Minnich, M. S. Dresselhaus, Z. F. Ren, G. Chen, *Energy Environ. Sci.* **2009**, *2*, 466–479.
[5] Y. Pei, H. Wang, G. J. Snyder, *Adv. Mater.* **2012**, *24*, 6124–6135.
[6] Y. Pei, X. Shi, A. LaLonde, H. Wang, L. Chen, G. J. Snyder, *Nature* **2011**, *473*, 66–69.
[7] K. S. Weldert, W. G. Zeier, T. W. Day, M. Panthöfer, G. J. Snyder, W. Tremel, *J. Am. Chem. Soc.* **2014**, *136*, 12035–12040.
[8] H. Liu, X. Shi, F. Xu, L. Zhang, W. Zhang, L. Chen, Q. Li, T. Day, G. J. Snyder, *Nat. Mater.* **2012**, *11*, 422–425.
[9] S. M. Kauzlarich, S. R. Brown, G. J. Snyder, *Dalton Trans.* **2007**, 2099–2107.
[10] G. Nolas, J. Cohn, J. Dyck, C. Uher, J. Yang, *Phys. Rev. B* **2002**, *65*, 1–6.
[11] B. Sales, D. Mandrus, R. Williams, *Science* **1996**, *272*, 1325–1328.
[12] E. S. Toberer, M. Christensen, B. Iversen, G. Snyder, *Phys. Rev. B* **2008**, *77*, 075203.
[13] E. S. Toberer, A. F. May, G. J. Snyder, *Chem. Mater.* **2010**, *22*, 624–634.
[14] D. Chung, T. Hogan, P. Brazis, M. Rocci-Lane, C. Kannewurf, M. Bastea, C. Uher, M. G. Kanatzidis, *Science* **2000**, *287*, 1024–1027.
[15] F. J. DiSalvo, *Science* **1999**, *285*, 703–706.
[16] H. J. Goldsmid, *Applications of Thermoelectricity*, Butler & Tanner, London, **1960**.
[17] A. D. LaLonde, Y. Pei, H. Wang, G. J. Snyder, *Mater. Today* **2011**, *14*, 526–532.

[18] G. S. Nolas, J. Poon, M. G. Kanatzidis, *MRS Bull.* **2006**, *31*, 199 – 205.
[19] Y. Pei, A. D. LaLonde, H. Wang, G. J. Snyder, *Energy Environ. Sci.* **2012**, *5*, 7963 – 7969.
[20] G. J. Snyder, E. S. Toberer, *Nat. Mater.* **2008**, *7*, 105 – 114.
[21] J. R. Sootsman, D. Y. Chung, M. G. Kanatzidis, *Angew. Chem. Int. Ed.* **2009**, *48*, 8616 – 8639; *Angew. Chem.* **2009**, *121*, 8768 – 8792.
[22] C. Wood, *Rep. Prog. Phys.* **1988**, *51*, 459 – 539.
[23] J. He, M. G. Kanatzidis, V. P. Dravid, *Mater. Today* **2013**, *16*, 166 – 176.
[24] L.-D. Zhao, V. P. Dravid, M. G. Kanatzidis, *Energy Environ. Sci.* **2014**, *7*, 251 – 268.
[25] H. Wang, Y. Pei, A. D. Lalonde, G. J. Snyder in *Thermoelectr. Nanomater. Springer Ser. Mater. Sci. 182* (Eds.: K. Koumoto, T. Mori), Springer, Berlin, **2013**, pp. 3 – 32.
[26] M. G. Kanatzidis, *Chem. Mater.* **2010**, *22*, 648 – 659.
[27] G. S. Pomrehn, A. Zevalkink, W. G. Zeier, A. van de Walle, G. J. Snyder, *Angew. Chem. Int. Ed.* **2014**, *53*, 3422 – 3426; *Angew. Chem.* **2014**, *126*, 3490 – 3494.
[28] E. S. Toberer, S. R. Brown, T. Ikeda, S. M. Kauzlarich, G. J. Snyder, *Appl. Phys. Lett.* **2008**, *93*, 062110.
[29] A. Zevalkink, G. S. Pomrehn, S. Johnson, J. Swallow, Z. M. Gibbs, G. Je, *Chem. Mater.* **2012**, *24*, 2091 – 2098.
[30] A. Zevalkink, E. S. Toberer, T. Bleith, E. Flage-Larsen, G. J. Snyder, *J. Appl. Phys.* **2011**, *110*, 013721.
[31] A. Zevalkink, E. S. Toberer, W. G. Zeier, E. Flage-Larsen, G. J. Snyder, *Energy Environ. Sci.* **2011**, *4*, 510 – 518.
[32] A. Zevalkink, W. G. Zeier, G. Pomrehn, E. Schechtel, W. Tremel, G. J. Snyder, *Energy Environ. Sci.* **2012**, *5*, 9121 – 9128.
[33] A. Zevalkink, W. G. Zeier, E. Cheng, G. J. Snyder, J.-P. Fleurial, S. Bux, *Chem. Mater.* **2014**, *26*, 5710 – 5717.
[34] Y. Pei, Z. M. Gibbs, A. Gloskovskii, B. Balke, W. G. Zeier, G. J. Snyder, *Adv. Energy Mater.* **2014**, *4*, 1400486.
[35] H. J. Goldsmid, *Thermoelectric Refrigeration*, Plenum, New York, **1964**.
[36] K. Burdett, *Prog. Solid State Chem.* **1984**, *15*, 173 – 255.
[37] R. Hoffmann, *Angew. Chem.* **1987**, *99*, 871 – 906.
[38] M.-H. Whangbo, E. Canadell, *Chem. Rev.* **1991**, *91*, 965 – 1034.
[39] G. S. Rohrer, *Structure and Bonding in Crystalline Materials*, Cambridge University Press, Cambridge, **2001**.
[40] W. A. Harrison, *Pure Appl. Chem.* **1989**, *61*, 2161 – 2169.
[41] T. Koopmans, *Physica* **1934**, *1*, 104 – 113.
[42] W. A. Harrison, *Phys. Rev. B* **1985**, *31*, 2121 – 2132.
[43] K. Li, Y. Li, D. Xue, *Funct. Mater. Lett.* **2012**, *05*, 1260002.
[44] P. A. Cox, *The Electronic Structure and Chemistry of Solids*, Oxford University Press, New York, **1987**.
[45] G. A. Slack in *Handb. Thermoelectr.* (Ed.: D. M. Rowe), CRC, Boca Raton, **1995**, pp. 407 – 440.
[46] D. J. Chadi, M. L. Cohen, *Phys. Status Solidi* **1975**, *68*, 405 – 419.
[47] H. Wang, J. Wang, X. Cao, G. J. Snyder, *J. Mater. Chem. A* **2014**, *2*, 3169 – 3174.
[48] R. J. Korkosz, T. C. Chasapis, S. Lo, J. W. Doak, Y. J. Kim, C. Wu, E. Hatzikraniotis, T. P. Hogan, D. N. Seidman, C. Wolverton, et al., *J. Am. Chem. Soc.* **2014**, *136*, 3225 – 3237.
[49] W. G. Zeier, C. P. Heinrich, T. Day, C. Panithipongwut, G. Kieslich, G. Brunklaus, G. J. Snyder, W. Tremel, *J. Mater. Chem. A* **2014**, *2*, 1790 – 1794.
[50] H. Wang, X. Cao, Y. Takagiwa, G. J. Snyder, *Mater. Horiz.* **2015**, *2*, 323 – 329.
[51] J. E. Jaffe, A. Zunger, *Phys. Rev. B* **1984**, *29*, 1882 – 1906.
[52] W. G. Zeier, J. Schmitt, G. Hautier, U. Aydemir, Z. M. Gibbs, C. Felser, G. J. Snyder, unpublished results.
[53] Y. P. Varshni, *Physica* **1967**, *34*, 149 – 154.
[54] Z. M. Gibbs, H. Kim, H. Wang, R. L. White, F. Drymiotis, M. Kaviany, G. J. Snyder, *Appl. Phys. Lett.* **2013**, *103*, 262109.
[55] K. Syassen, N. E. Christensen, H. Winzen, K. Fischer, J. Evers, *Phys. Rev. B* **1987**, *35*, 4052 – 4059.
[56] E. S. Bozin, C. D. Malliakas, P. Souvatzis, T. Proffen, N. A. Spaldin, M. G. Kanatzidis, S. J. L. Billinge, *Science* **2010**, *330*, 1660 – 1663.
[57] S. Kastbjerg, N. Bindzus, M. Søndergaard, S. Johnsen, N. Lock, M. Christensen, M. Takata, M. A. Spackman, B. B. Iversen, *Adv. Funct. Mater.* **2013**, *23*, 5477 – 5483.
[58] L. M. Schoop, L. Müchler, C. Felser, R. J. Cava, *Inorg. Chem.* **2013**, *52*, 5479 – 5483.
[59] M. Miao, J. Brgoch, A. Krishnapriyan, A. Goldman, J. A. Kurzman, R. Seshadri, *Inorg. Chem.* **2013**, *52*, 8183 – 8189.
[60] N. A. Spaldin, S. Cheong, R. Ramesh, *Phys. Today* **2010**, *63*, 38 – 34.
[61] B. B. Van Aken, T. T. M. Palstra, A. Filippetti, N. A. Spaldin, *Nat. Mater.* **2004**, *3*, 164 – 170.
[62] A. Walsh, D. J. Payne, R. G. Egdell, G. W. Watson, *Chem. Soc. Rev.* **2011**, *40*, 4455 – 4463.
[63] A. Walsh, G. W. Watson, *J. Solid State Chem.* **2005**, *178*, 1422 – 1428.
[64] U. Waghmare, N. Spaldin, H. Kandpal, R. Seshadri, *Phys. Rev. B* **2003**, *67*, 125111.
[65] S. N. Guin, V. Srihari, K. Biswas, *J. Mater. Chem. A* **2015**, *3*, 648 – 655.
[66] M. G. Kanatzidis in *Semicond. Semimetals. Recent Trends Thermoelectr. Mater. Res. I* (Ed.: T. M. Tritt), Elsevier, Amsterdam, **2001**, pp. 51 – 100.
[67] D. Parker, A. F. May, D. J. Singh, *arXiv* **2015**, *37831*, arXiv:1505.03379.
[68] D. Parker, X. Chen, D. J. Singh, *Phys. Rev. Lett.* **2013**, *110*, 146601.
[69] Z. M. Gibbs, H. Zhu, G. Li, G. Hautier, A. Jain, K. Persson, G. Ceder, G. J. Snyder, unpublished results.
[70] X. Chen, D. Parker, D. J. Singh, *Sci. Rep.* **2013**, *3*, 3168.
[71] N. A. Mecholsky, L. Resca, I. L. Pegg, M. Fornari, *Phys. Rev. B* **2014**, *89*, 155131.
[72] D. I. Bilc, G. Hautier, D. Waroquiers, G.-M. Rignanese, P. Ghosez, *Phys. Rev. Lett.* **2015**, *114*, 1 – 5.
[73] U. Waghmare, N. Spaldin, H. Kandpal, R. Seshadri, *Phys. Rev. B* **2003**, *67*, 164 – 170.
[74] R. F. Brebrick, A. J. Strauss, *Phys. Rev.* **1963**, *131*, 104 – 110.
[75] G. Tan, F. Shi, W. Doak, H. Sun, L. Zhao, *Energy Environ. Sci.* **2015**, *8*, 267 – 277.
[76] G. Tan, L. D. Zhao, F. Shi, J. W. Doak, S. H. Lo, H. Sun, C. Wolverton, V. P. Dravid, C. Uher, M. G. Kanatzidis, *J. Am. Chem. Soc.* **2014**, *136*, 7006 – 7017.
[77] G. Hautier, A. Miglio, G. Ceder, G.-M. Rignanese, X. Gonze, *Nat. Commun.* **2013**, *4*, 2292.
[78] Y. Pei, A. LaLonde, S. Iwanaga, G. J. Snyder, *Energy Environ. Sci.* **2011**, *4*, 2085 – 2089.
[79] A. Jain, S. P. Ong, G. Hautier, W. Chen, W. D. Richards, S. Dacek, S. Cholia, D. Gunter, D. Skinner, G. Ceder, et al., *APL Mater.* **2013**, *1*, 011002.
[80] J. Perdew, K. Burke, M. Ernzerhof, *Phys. Rev. Lett.* **1996**, *77*, 3865 – 3868.
[81] Y. Pei, A. D. LaLonde, N. A. Heinz, X. Shi, S. Iwanaga, H. Wang, L. Chen, G. J. Snyder, *Adv. Mater.* **2011**, *23*, 5674 – 5678.
[82] H. Wang, Z. M. Gibbs, Y. Takagiwa, G. J. Snyder, *Energy Environ. Sci.* **2014**, *7*, 804 – 811.
[83] Y. Lee, S.-H. Lo, J. Androulakis, C.-I. Wu, L.-D. Zhao, D.-Y. Chung, T. P. Hogan, V. P. Dravid, M. G. Kanatzidis, *J. Am. Chem. Soc.* **2013**, *135*, 5152 – 5160.
[84] L. D. Zhao, H. J. Wu, S. Q. Hao, C. I. Wu, X. Y. Zhou, K. Biswas, J. Q. He, T. P. Hogan, C. Uher, C. Wolverton, et al., *Energy Environ. Sci.* **2013**, *6*, 3346 – 3355.
[85] M. Zhou, Z. M. Gibbs, H. Wang, Y. Han, C. Xin, L. Li, G. J. Snyder, *Phys. Chem. Chem. Phys.* **2014**, *16*, 20741 – 20748.

[86] H. Zhu, W. Sun, R. Armiento, P. Lazic, G. Ceder, *Appl. Phys. Lett.* **2014**, *104*, 082107.
[87] J. Zhang, R. Liu, N. Cheng, Y. Zhang, J. Yang, C. Uher, X. Shi, L. Chen, W. Zhang, *Adv. Mater.* **2014**, *26*, 3848 – 3853.
[88] W. G. Zeier, H. Zhu, Z. M. Gibbs, G. Ceder, W. Tremel, G. J. Snyder, *J. Mater. Chem. C* **2014**, *2*, 10189 – 10194.
[89] W. Liu, X. Tan, K. Yin, H. Liu, X. Tang, J. Shi, Q. Zhang, C. Uher, *Phys. Rev. Lett.* **2012**, *108*, 166601.
[90] V. K. Zaitsev, E. N. Tkalenko, E. N. Nikitin, *Sov. Phys. Solid State* **1969**, *11*, 221 – 224.
[91] H.-S. Kim, Z. M. Gibbs, Y. Tang, H. Wang, G. J. Snyder, *APL Mater.* **2015**, *3*, 041506.
[92] G. Liebfried, E. Schlöhmann, *Nachr. Akad. Wiss. Göttingen Math. Phys. Kl.* **1954**, *4*, 71.
[93] G. A. Slack, *J. Phys. Chem. Solids* **1973**, *34*, 321 – 335.
[94] P. G. Klemens in *Thermal Conductivity* (Ed.: R. P. Tye), Acdemic Press, London, **1969**.
[95] C. L. Julian, *Phys. Rev.* **1965**, *137*, A128 – A137.
[96] E. S. Toberer, A. Zevalkink, G. J. Snyder, *J. Mater. Chem.* **2011**, *21*, 15843 – 15852.
[97] A. F. May, G. J. Snyder in *Thermoelectrics Handbook: Thermoelectrics and its Energy Harvesting* (Ed.: D. M. Rowe), CRC, Boca Raton, **2012**.
[98] A. V. Ioffe, *Sov. Phys. Solid State* **1963**, *5*, 2446 – 2447.
[99] D. P. Spitzer, *J. Phys. Chem. Solids* **1970**, *31*, 19 – 40.
[100] J. Yang in *Therm. Conduct. Prop. Appl.* (Ed.: T. M. Tritt), Kluwer/Plenum, New York, **2004**, pp. 1 – 20.
[101] L. Garbato, A. Rucci, *Chem. Phys. Lett.* **1979**, *61*, 542 – 544.
[102] "High lattice thermal conductivity in solids": D. T. Morelli, G. A. Slack in High Thermal Conductivity in Materials, Springer, New York, **2005**, pp. 37 – 64.
[103] G. D. Khattak, H. Akbarzadeh, P. H. Keesom, *Phys. Rev. B* **1981**, *23*, 2911 – 2915.
[104] G. A. Slack, *Solid State Physics*, Academic Press, New York, **1979**.
[105] L. Cohen, *Phys. Rev. B* **1985**, *32*, 7988 – 7991.
[106] D. H. Parkinson, J. E. Quarrington, *Proc. Phys. Soc.* **1954**, *67*, 569 – 579.
[107] H. Wang, Y. Pei, A. D. Lalonde, G. J. Snyder, *Adv. Mater.* **2011**, *23*, 1366 – 1370.
[108] P. D. Maycock, *Solid-State Electron.* **1967**, *10*, 161.
[109] E. F. Steigmeier, I. Kudman, *Phys. Rev.* **1963**, *132*, 508 – 512.
[110] E. Steigmeier, I. Kudman, *Phys. Rev.* **1966**, *141*, 767 – 774.
[111] E. F. Steigmeier, B. Abeles, *Phys. Rev.* **1964**, *136*, 1149 – 1155.
[112] M. G. Holland, *Phys. Rev.* **1964**, *134*, A471 – A480.
[113] A. V. Ioffe, A. F. Ioffe, *Sov. Phys. Solid State* **1960**, *2*, 719 – 728.
[114] A. I. Zaslavskii, V. M. Sergeeva, I. A. Smirnov, *Sov. Phys. Semicond.* **1961**, *2*, 2565.
[115] H. Weiss, *Ann. Phys.* **1959**, *4*, 121 – 124.
[116] A. Amith, I. Kudman, E. F. Steigmeier, *Phys. Rev.* **1965**, *138*, A1270 – A1276.
[117] E. I. Gavrilitsa, S. I. Radautsan, *Phys. Status Solidi* **1967**, *19*, 609 – 611.
[118] R. O. Carlson, *Phys. Rev.* **1958**, *111*, 476 – 478.
[119] I. Kudman, E. F. Steigmeier, *Phys. Rev.* **1964**, *122*, A1665 – A1667.
[120] G. Busch, E. F. Steigmeier, *Helv. Phys. Acta* **1961**, *34*, 1 – 28.
[121] F. D. Rosi, E. F. Hockings, N. E. Lindenbald, *RCA Rev.* **1961**, *22*, 82 – 121.
[122] E. D. Devyatkova, V. P. Zhuze, A. V. Golubkov, V. M. Sergeeva, I. A. Smirnov, *Sov. Phys. Solid State* **1964**, *6*, 343 – 346.
[123] R. A. H. Hamilton, J. E. Parrott, *Phys. Lett.* **1969**, *29*, 29 – 31.
[124] B. Xu, Q. Wang, Y. Tian, *Sci. Rep.* **2013**, *3*, 3068.
[125] G. V. Gibbs, F. C. Hill, M. B. Boisen, R. T. Downs, *Phys. Chem. Miner.* **1998**, *25*, 585 – 590.
[126] W. Grochala, R. Hoffmann, J. Feng, N. W. Ashcroft, *Angew. Chem. Int. Ed.* **2007**, *46*, 3620 – 3642; *Angew. Chem.* **2007**, *119*, 3694 – 3717.
[127] I. D. Brown, R. D. Shannon, *Acta Crystallogr. Sect. A* **1973**, *29*, 266 – 282.
[128] L. D. Dudkin, A. P. Ostranitza, *Dokl. Akad. Nauk SSSR* **1959**, *124*, 94.
[129] D. B. Gasson, P. J. Holmes, I. C. Jennings, B. R. Marathe, J. E. Parrott, *J. Phys. Chem. Solids* **1962**, *23*, 1291.
[130] E. F. Hockings, *J. Phys. Chem. Solids* **1959**, *10*, 341.
[131] K. Masumoto, S. Isomura, W. Goto, *J. Phys. Chem. Solids* **1966**, *27*, 1939.
[132] A. V. Petrov, E. L. Shtrum, *Sov. Phys. Solid State* **1962**, *4*, 1061.
[133] F. D. Rosi, J. P. Dismukes, E. F. Hockings, *Electr. Eng.* **1960**, *79*, 450.
[134] S. M. Zalar, I. B. Cadoff, *Trans. AIME* **1962**, *224*, 436.
[135] R. J. Gummow, I. Sigalas, *Int. J. Thermophys.* **1987**, *8*, 607 – 620.
[136] R. W. Keyes, *Phys. Rev.* **1959**, *115*, 564 – 567.
[137] S. Lee, K. Esfarjani, T. Luo, J. Zhou, Z. Tian, G. Chen, *Nat. Commun.* **2014**, *5*, 3525.
[138] L. Pauling, *J. Am. Chem. Soc.* **1929**, *51*, 1010 – 1026.
[139] F. C. Hawthorne, *Acta Crystallogr. Sect. B* **1994**, *50*, 481 – 510.
[140] D. K. C. MacDonald, S. K. Roy, *Phys. Rev.* **1955**, *97*, 673 – 676.
[141] J. Yan, P. Gorai, B. Ortiz, S. Miller, S. A. Barnett, T. Mason, E. S. Toberer, *Energy Environ. Sci.* **2015**, *8*, 983 – 994.
[142] D. T. Morelli, V. Jovovic, J. P. Heremans, *Phys. Rev. Lett.* **2008**, *101*, 16 – 19.
[143] M. D. Nielsen, V. Ozolins, J. P. Heremans, *Energy Environ. Sci.* **2013**, *6*, 570 – 578.
[144] E. Skoug, D. Morelli, *Phys. Rev. Lett.* **2011**, *107*, 235901.
[145] W. Lai, Y. Wang, D. T. Morelli, X. Lu, *Adv. Funct. Mater.* **2015**, *25*, 3648 – 3657.
[146] Y. Zhang, E. Skoug, J. Cain, V. Ozoliņš, D. Morelli, C. Wolverton, *Phys. Rev. B* **2012**, *85*, 054306.
[147] a) L.-D. Zhao, S.-H. Lo, Y. Zhang, H. Sun, G. Tan, C. Uher, C. Wolverton, V. P. Dravid, M. G. Kanatzidis, *Nature* **2014**, *508*, 373 – 377; b) L.-D. Zhao, G. Tan, S. Hao, J. He, Y. Pei, H. Chi, H. Wang, S. Gong, H. Xu, V. P. Dravid, C. Uher, G. J. Snyder, C. Wolverton, M. G. Kanatzidis, *Science*, **2016**, *351*, 141 – 144.
[148] S. Johnsen, J. He, J. Androulakis, V. P. Dravid, I. Todorov, D. Y. Chung, M. G. Kanatzidis, *J. Am. Chem. Soc.* **2011**, *133*, 3460 – 3470.
[149] Y. Pei, N. A. Heinz, A. LaLonde, G. J. Snyder, *Energy Environ. Sci.* **2011**, *4*, 3640 – 3645.
[150] P. F. P. Poudeu, J. D'Angelo, A. D. Downey, J. L. Short, T. P. Hogan, M. G. Kanatzidis, *Angew. Chem. Int. Ed.* **2006**, *45*, 3835 – 3839; *Angew. Chem.* **2006**, *118*, 3919 – 3923.
[151] M. Zebarjadi, K. Esfarjani, M. S. Dresselhaus, Z. F. Ren, G. Chen, *Energy Environ. Sci.* **2012**, *5*, 5147 – 5162.
[152] W. G. Zeier, A. LaLonde, Z. M. Gibbs, C. P. Heinrich, M. Panthöfer, G. J. Snyder, W. Tremel, *J. Am. Chem. Soc.* **2012**, *134*, 7147 – 7154.
[153] W. G. Zeier, A. Zevalkink, E. Schechtel, W. Tremel, G. J. Snyder, *J. Mater. Chem.* **2012**, *22*, 9826 – 9830.
[154] G. Kieslich, I. Veremchuk, I. Antonyshyn, W. G. Zeier, C. S. Birkel, K. Weldert, C. P. Heinrich, E. Visnow, M. Panthöfer, U. Burkhardt, et al., *Phys. Chem. Chem. Phys.* **2013**, *15*, 15399 – 15403.
[155] J. Callaway, H. C. Baeyer, *Phys. Rev.* **1960**, *120*, 1149 – 1154.
[156] J. Callaway, *Phys. Rev.* **1959**, *113*, 1046 – 1051.
[157] J. Yang, G. P. Meisner, L. Chen, *Appl. Phys. Lett.* **2004**, *85*, 1140 – 1142.
[158] Z. Zhou, C. Uher, A. Jewell, T. Caillat, *Phys. Rev. B* **2005**, *71*, 235209.
[159] G. Meisner, D. Morelli, S. Hu, J. Yang, C. Uher, *Phys. Rev. Lett.* **1998**, *80*, 3551 – 3554.

[160] G. T. Alekseeva, B. A. Efimova, L. M. Ostrovskaya, O. S. Serebryannikova, M. I. Tsypin, *Sov. Phys. Semicond.* **1971**, *4*, 1122 – 1125.
[161] B. Abeles, *Phys. Rev.* **1963**, *131*, 1906 – 1911.
[162] B. R. Ortiz, H. Peng, A. Lopez, P. A. Parilla, S. Lany, E. S. Toberer, *Phys. Chem. Chem. Phys.* **2015**, *17*, 19410 – 19423.
[163] P. G. Klemens, *Proc. Phys. Soc.* **1955**, *68*, 1113 – 1128.
[164] F. Gascoin, S. Ottensmann, D. Stark, S. M. Haile, G. J. Snyder, *Adv. Funct. Mater.* **2005**, *15*, 1860 – 1864.
[165] E. S. Toberer, A. F. May, B. C. Melot, E. Flage-Larsen, G. J. Snyder, *Dalton Trans.* **2010**, *39*, 1046 – 1054.
[166] C. P. Heinrich, T. W. Day, W. G. Zeier, G. J. Snyder, W. Tremel, *J. Am. Chem. Soc.* **2014**, *136*, 442 – 448.
[167] H. Wang, J. Wang, X. Cao, G. J. Snyder, *J. Mater. Chem. A* **2014**, *2*, 3169 – 3174.
[168] W. G. Zeier, Y. Pei, G. Pomrehn, T. Day, N. A. Heinz, C. P. Heinrich, G. J. Snyder, W. Tremel, *J. Am. Chem. Soc.* **2013**, *135*, 726 – 732.
[169] Y. Li, T. Zhang, Y. Qin, T. Day, G. J. Snyder, X. Shi, L. Chen, *J. Appl. Phys.* **2014**, *116*, 203705.
[170] P. K. de Boer, *Am. J. Phys.* **1999**, *67*, 443 – 445.

Received: September 7, 2015
Published online: April 25, 2016

